Luminescence characteristics and energy transfer in the mixed $Y_xGd_{1-x}F_3$:Ce, Me (Me = Mg, Ca, Sr, Ba) crystals

2006 J. Phys.: Condens. Matter 18 3069

(http://iopscience.iop.org/0953-8984/18/11/012)

INSTITUTE OF PHYSICS PUBLISHING JOURNAL OF PHYSICS: CONDENSED MATTER

J. Phys.: Condens. Matter **18** (2006) 3069–3079 doi:10.1088/0953-8984/18/11/012

Luminescence characteristics and energy transfer in the mixed $Y_xGd_{1-x}F_3$:Ce, Me (Me = Mg, Ca, Sr, Ba) crystals

M Nikl[1,4], K Kamada[2], A Yoshikawa[2], A Krasnikov[3], A Beitlerova[1], N Solovieva[1], J Hybler[1] and T Fukuda[2]

[1] Institute of Physics AS CR, Cukrovarnicka 10, 16253 Prague, Czech Republic
[2] Institute of Multidisciplinary Research for Advanced Materials, Tohoku University, 2-1-1 Katahira, Aoba-ku, Sendai 980-8577, Japan
[3] Institute of Physics, University of Tartu, Riia 142, 51014 Tartu, Estonia

E-mail: nikl@fzu.cz

Received 12 December 2005
Published 1 March 2006
Online at stacks.iop.org/JPhysCM/18/3069

Abstract

The luminescence spectra and decay kinetics are measured within 80–300 K for the set of mixed YF_3–GdF_3 single-crystal fluoride hosts doped by the Ce^{3+} and Me^{2+} (Me = Mg, Ca, Sr, Ba) ions. For certain Ce and Me concentration ranges we observe creation of the Ce^{3+}-distorted luminescence centre with the emission maximum around 380–390 nm. Energy migration through the Gd sublattice and a transfer to the Ce^{3+}-distorted centre is evidenced and modelled using a simple Stern–Volmer approximation.

1. Introduction

Luminescence characteristics of the Ce^{3+} centres in fluoride hosts were studied in a number of compounds. The position and arrangement of the 5d excited level were systematically analysed; see [1, 2] and references therein. The Ce^{3+} emission centre in fluoride hosts is of interest for practical applications due to its high quantum efficiency at room temperature and broad emission spectrum in UV, that can be used for development of tunable, short pulse, solid state lasers in this spectral region [3–5]. Furthermore, fast scintillation materials have been searched for within Ce-doped fluorides as well. Namely, it is worth mentioning extended studies on CeF_3 (see [6] for review), Ce-doped $LiREF_4$ [7] and $BaRE_2F_8$ [8] (RE = Y, Lu) single crystals.

In the group of crystalline or glassy halides and oxides one has been systematically searching for compounds manifesting an overlap between the ^8S–^6P transition of Gd^{3+} and some of the 4f–5d absorption bands of Ce^{3+}. Such an arrangement can facilitate an efficient host-to-activator energy transfer in the Ce-doped and Gd-based compounds [9, 10]; see [11]

[4] Author to whom any correspondence should be addressed.

for an overview of this strategy in scintillator research. Energy migration via the Gd sublattice inevitably introduces slow components in the scintillation decay. However, in the case of Gd-dense compounds and high Ce^{3+} concentration, as fast as submicrosecond slow-component decay times were achieved, e.g. in $RbGd_2Br_7$:Ce [12] or Gd_2SiO_5:Ce [9]. Due to the weaker crystal field in fluorides, comparing to other compounds, in the most frequent situation even the lowest energy $4f–5d^1$ absorption band of Ce^{3+} is energetically higher than the $^6P–^8S$ transition of Gd^{3+}. Therefore, the above concept does not work, as in $LiGdF_4$:Ce [13]. In a more favourable case, the bidirectional energy transfer $Gd^{3+} \leftrightarrow Ce^{3+}$ occurs, like in $CsGd_2F_7$:Ce [14]. Nevertheless, the back energy transfer slows down the overall scintillation response of the material.

In binary fluoride compounds such as GdF_3, LaF_3, LuF_3 or CeF_3 the lowest $4f–5d^1$ absorption transition of Ce^{3+} is positioned around 250–260 nm and the related emission peaks at 290–310 nm, i.e. the reverse Ce^{3+}–Gd^{3+} energy transfer is also realized [15–18]. However, in some cases there is an efficient creation of so called 'perturbed Ce' centres that are associated with the emissions of somewhat lower energy shifted towards 340–350 nm with excitation bands occurring around 270–280 nm [15, 18]. The oxygen contamination [15] or more probably fluorine vacancy were considered [18–20] as the perturbing agents. The mutual position and overlap of the absorption and emission bands related to regular and perturbed Ce^{3+}, Tb^{3+}, or Mn^{2+} centres with those of the Gd^{3+} ions enable the following energy transfer process: regular $Ce^{3+} \rightarrow (Gd^{3+}–Gd^{3+} \cdots –Gd^{3+})_n \rightarrow$ perturbed $Ce^{3+}(Tb^{3+}, Mn^{2+})$. These phenomena were described in the literature in a number of papers [15, 21, 22] as such compositions appeared favourable in the research on phosphors in lighting applications.

In the present paper we introduce a modified mixed fluoride host based on a YF_3–GdF_3 single crystal. A Ce-distorted centre can be created using a codoping by selected divalent ions. Such a centre shows enhanced Stokes shift and its emission peaks at about 380–390 nm. An efficient energy transfer from the Gd sublattice to Ce^{3+} centres occurs and no back energy transfer to the Gd sublattice is detected even at room temperature. The energy migration process and concentration dependence of the donor Gd^{3+} emission is successfully described in terms of a simple Stern–Volmer approximation.

2. Experimental details

Rod-shaped single crystals of mixed YF_3–GdF_3 binary fluorides, further doped by CeF_3 and MeF_2 (Me = Mg, Ca, Sr, Ba), were grown by the micro-pulling-down method under a protective atmosphere; see [23] for more detailed description of the growth technique. Starting materials were prepared from the stoichiometric mixture of 99.99% pure CeF_3, YF_3, GdF_3 and MeF_2 (Me = Mg, Ca, Sr, Ba) powders produced by Stella Chemifa Corporation. We further denote the codoped samples by indicating the percentage of binary fluorides (except GdF_3) in the starting powder mixture. Powders were well mixed and put into a carbon crucible. First, the chamber was evacuated up to 10^{-3} Torr, then the crucible was heated up to 500 °C. In order to remove a possible oxygen source such as moisture of raw materials and chamber surface, it was kept at this temperature for about 1 h. During this baking procedure, the chamber was evacuated up to 10^{-4} Torr. After the baking, vacuum system was stopped and high purity CF_4 (99.999%) was let into the chamber. Then, under ambient pressure, the crucible was heated up to melting temperature (∼1250 °C). A $Gd_{0.5}Y_{0.5}F_3$ single crystal was used as a seed for the initial crystal growth. The growth rate was 0.16 mm min^{-1}. The prepared compositions are listed in table 1.

Dimensions of the rods were typically ⌀ 2 mm × 40 mm. They were transparent, crackless and without visible inclusions. The percentage of YF_3 and GdF_3 constituents was determined to achieve a stable congruent growth of the beta-YF_3 structure with D_{2h}^{16}-*Pnma* symmetry

Table 1. List of the prepared samples and their radioluminescence intensity at 310 and 380 nm at RT.

Composition	RL intensity at 310 nm	RL intensity at 380 nm
Y50%GdF_3	Very high	Zero
Ce1%Y50%GdF_3	Very high	Zero
Ce5%Y30%GdF_3	Very high	Very low
Mg0.5%Ce3%Y60%GdF3	Very high	Zero
Ca0.5%Ce5%Y60%GdF3	Low	Very high
Ca0.5%Ce8%Y60%GdF3	Low	High
Ca1%Ce3%Y60%GdF3	Medium	High
Ca1.5%Ce3%Y60%GdF3	Medium	High
Sr0.1%Ce1%Y55%GdF3	Medium	Medium–high
Sr3%Ce3%Y49%GdF3	Low	Very high
Sr7%Ce15%GdF3	Medium	Medium
Ba3%Ce3%Y49%GdF3	Medium	Low

(DyF_3 like); the details will be published in a separate paper [24]. Routine x-ray structural diagnostics was applied to all the samples grown: part of each was powdered for this purpose. The beta-YF_3 structure was confirmed and no other parasitic structural phase was revealed. Plates of about 2 mm × 8 mm × 1 mm were cut and polished for the absorption and luminescence measurements.

Absorption spectra were measured with UV–VIS–NIR spectrophotometer Shimadzu UV-3101PC at room temperature (RT). Measurements of photoluminescence were performed within 80–400 K using liquid nitrogen bath optical cryostats of Oxford Instrument. A Spectrofluorometer 199S (Edinburgh Instruments) was used for the luminescence experiment. It was equipped with a steady-state hydrogen flash-lamp, pulsed xenon microsecond flash-lamp, nanosecond hydrogen-filled flash-lamp and an x-ray tube as the excitation sources. A single-grating emission monochromator and Peltier-cooled TBX-04 detection module (IBH Scotland) working in photon counting mode were used in the detection part. All the spectra were corrected for experimental distortions. Luminescence decay kinetics within ns–ms timescale was measured in the same set-up using (i) the microsecond xenon flash-lamp and detection by a multichannel analyser in the scaling mode for slow decay processes and (ii) the nanosecond hydrogen-filled coaxial flash-lamp and time-correlated single-photon counting method for fast nanosecond decay processes. Deconvolution procedures (Spectra-Solve software of LASTEK Ltd) were used to extract true decay times in the situation when the decay curves were distorted due to a finite width of the instrumental response.

3. Experimental results

Figure 1 shows the absorption spectra of selected compositions. In the region of 310 nm one observes a typical absorption related to the transition from the $^8S_{7/2}$ ground state to the ^6P multiplet of the Gd^{3+} ion. Towards shorter wavelengths there is a region of variable absorption (see the inset in which the curves were around 318 nm set to approximately the same ordinate value) finally followed by the onset of the $4f–5d^1$ absorption band of Ce^{3+} below 280 nm. Some samples manifest an additional light scattering, smoothly increasing absorption towards shorter wavelengths (curve (b) in figure 1).

Radioluminescence (RL) spectra under non-resonant excitation by x-rays in figure 2 show at RT the expected Gd^{3+} emission around 310 nm and another wide emission band at 380–390 nm, the intensity of which is strongly varying with the sample composition; see also table 1.

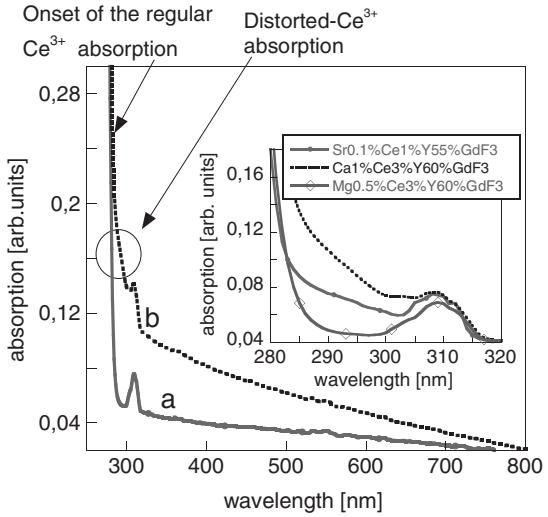

Figure 1. Room temperature absorption spectra of the sample with the composition Mg.5%Ce3%Y60%GdF3 (a) and Ca1%Ce3%Y60%GdF3 (b). In the inset the enlarged absorption spectra within 280–320 nm (vertically shifted to the same ordinate value at 318 nm) are given for three representative samples with compositions given in the legend.

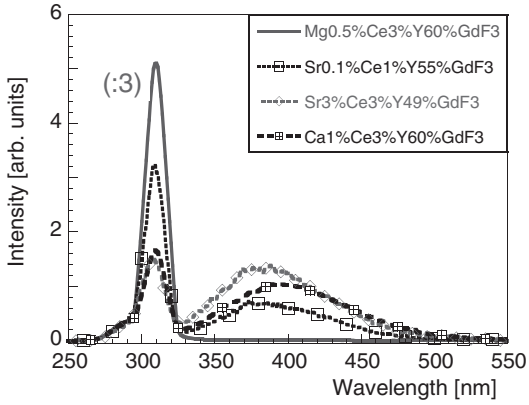

Figure 2. Radioluminescence spectra (x-ray tube, 28 kV) at room temperature, sample compositions are in the legend. Spectra are mutually comparable in an absolute way.

In the Ce-containing samples the room temperature excitation spectra of both the 310 and 380 nm bands below 280 nm coincide (see figure 3), while above this wavelength they are clearly different. The difference spectrum (curve c) peaks at 290 nm and its low energy tail features a definite fingerprint of the Gd^{3+} ^8S–$^6P_{5/2,7/2}$ absorption transitions. The peak of the excitation spectra around 275 nm coincides with the position of the ^8S–^6I absorption transition of Gd^{3+}. In the samples where RL measurement shows the presence of the 380 nm band (figure 2) the emission spectrum under excitation at 275 nm is qualitatively similar, i.e. containing both the 310 and 380 nm bands. An example is included in figure 3, (curve d).

In the Ca1%Ce3%Y60%GdF_3 sample we measured and evaluated the temperature dependence of photoluminescence intensity under both the 272 and 311 nm excitations.

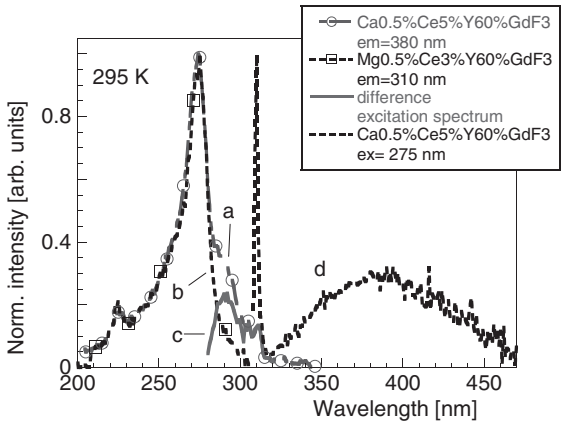

Figure 3. Excitation ((a), (b)), difference excitation (c) and emission (d) spectra at room temperature. Compositions, excitation and emission wavelengths are in the legend.

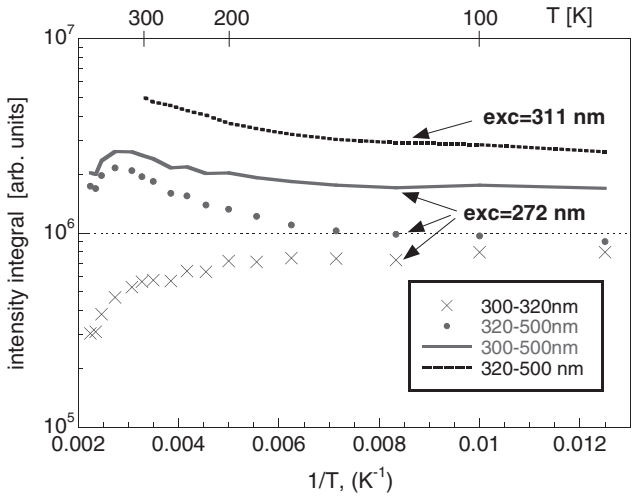

Figure 4. Temperature dependence of the emission spectra of the Ca1%Ce3%Y60%GdF3 sample; the excitation wavelength is marked in the figure. Obtained values are the integrated spectra within the intervals given in the legend.

Namely, the integral of the measured photoluminescence spectra was calculated for each temperature and its temperature dependence is displayed in figure 4. Under the 272 nm excitation a clear evidence of energy transfer from the 310 to 380 nm band was obtained with increasing temperature (300–320 nm and 320–500 nm integrals). It is interesting to note that the total intensity (300–500 nm integral) is slightly increasing with temperature especially above 200 K. Similarly, an increasing emission intensity is obtained under the 311 nm excitation for the 380 nm band (320–500 nm integral).

Furthermore, the slow decay kinetics of the 310 nm emission band was measured at RT using the microsecond xenon flash-lamp excitation. For the 310 nm emission decay the longest decay times are obtained in the samples where the 380 nm band is absent. A decay time of about 13–14 ms was evaluated; see figure 5. With increasing 380 nm emission intensity (monitored by RL measurement, see figure 2 and table 1) the decay time of the 310 nm band decreases to

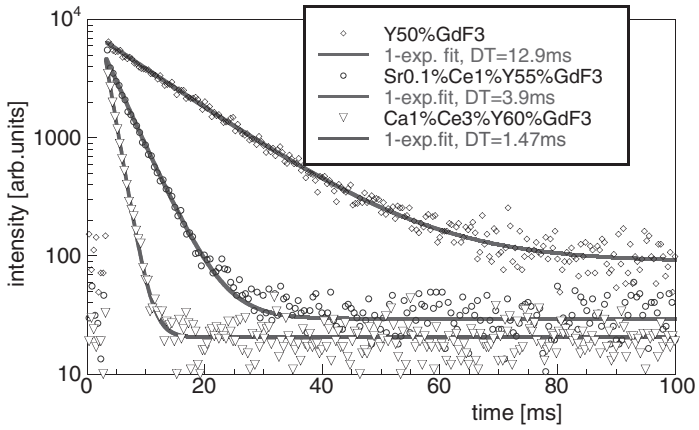

Figure 5. Photoluminescence decays of selected compositions given in the legend, $\lambda_{exc} = 275$ nm, $\lambda_{em} = 311$ nm, $T = 295$ K. Experimental data are given by symbols. The solid line is the single-exponential approximation ($I(t) = A\exp[-t/\tau]+$ background) with the value of decay time τ given in the legend as the DT parameter.

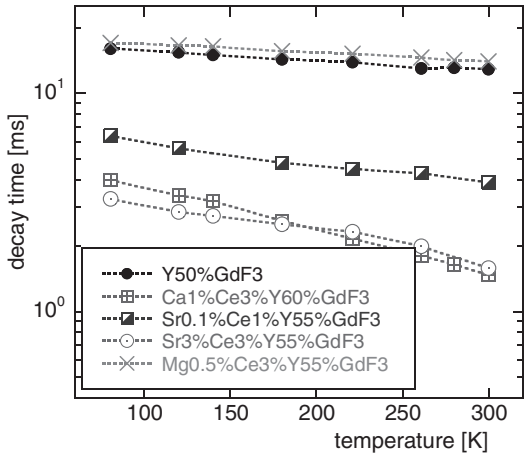

Figure 6. Temperature dependence of the 310 nm emission decay times obtained from a single-exponential approximation, similarly as in figure 5. Decay curves are measured under the resonant excitation $\lambda_{exc} = 310$ nm.

about 1.5 ms in Ca1%Ce3%Y60%GdF_3 or Sr3%Ce3%Y55%GdF_3 samples. Such behaviour is consistent with the observed energy transfer process in figure 4. It is worth noting the perfect single-exponential course of all three decay curves in figure 5, which was found at RT for all the samples studied.

Using the single-exponential approximation $I(t) = A \cdot \exp[-t/\tau]+$ background, the decay times τ were evaluated from the decay curves at several temperatures within 80–300 K for several samples with varying RL intensity of the 380 nm band, see figure 6. There is a straightforward correlation between increasing RL intensity of the 380 nm band at RT and decreasing value of the decay times over the whole temperature range. Furthermore, in the samples with an intense 380 nm band there is a steeper temperature dependence of the decay times within 80–300 K.

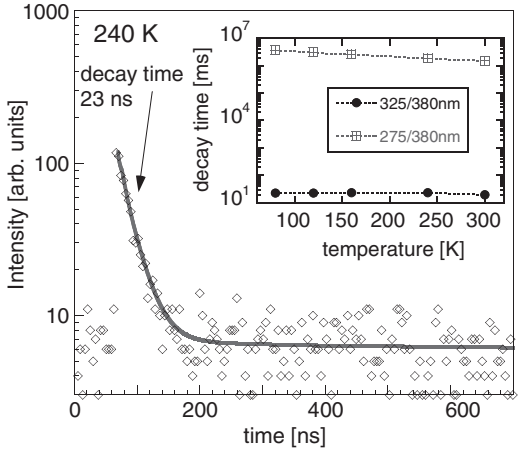

Figure 7. Photoluminescence decay of the 380 nm band under excitation $\lambda_{exc} = 325$ nm, $T = 240$ K. The solid line is the convolution of the instrumental function (not in the figure) and a single-exponential function $I(t) = A\exp[-t/\tau] +$ background. In the inset the values of decay times are given within 80–300 K range under two different excitation wavelengths.

Finally, decay curves were measured for the 380 nm emission under both the 275 and 325 nm excitations. While the former excitation is tuned in the spectral region where the absorption of the Gd^{3+} (^8S–^6I) and Ce^{3+} ($4f$–$5d^1$) are overlapped, the latter excitation is already below the lowest energy ^8S–^6P absorption transition of Gd^{3+}. Using the microsecond xenon flash-lamp excitation at 275 nm the decay curve at 380 nm closely resembles that observed at 310 nm. The evaluated millisecond decay time values are practically the same; see the inset of figure 7 for the sample Ca1%Ce3%Y60%GdF_3. In contrast, the nanosecond flash-lamp excitation at 325 nm gives rise to a fast 380 emission with the single-exponential decay as well. Evaluated decay time shows the values typical for the 5d–4f luminescence of Ce^{3+}, see an example at 240 K in figure 7. Within 80–300 K, the decay time values of about 19–23 ns were obtained, see the inset of figure 7. No slower decay components were observed in the 380 nm band under the 325 nm excitation using both mentioned pulse excitation flash-lamps.

4. Discussion

In the present case the regular Ce^{3+} centres are manifested by a weak emission shoulder around 285–290 nm (figure 2). Under excitation around 250 nm the decay time of this emission band is of the order of only 1–1.5 ns. Such a short decay time and low emission intensity is fully coherent with an earlier given hypothesis of energy transfer from this centre towards the Gd^{3+} cationic sublattice [15] also in this material system. This explanation is further supported by the shape of the 310 nm band excitation spectrum in figure 3, showing noticeable intensity also outside the Gd^{3+}-related absorption transitions situated around 200–210 nm (to ^6G multiplet), 240–250 nm (to ^6D multiplet) and 270–275 nm (to ^6I multiplet).

In the samples where the 380 nm band is absent, the obtained decay times of the 310 nm emission of Gd^{3+} are very long and with relatively weak temperature dependence. Simultaneous decay time decrease and emission intensity transfer into the 380 nm band undoubtedly evidence the energy transfer from the 310 to 380 nm bands, which is also well supported by the shape of the low energy part of the 380 nm band excitation spectrum (difference spectrum in figure 3) extended to 330 nm. Further support comes from the fact that

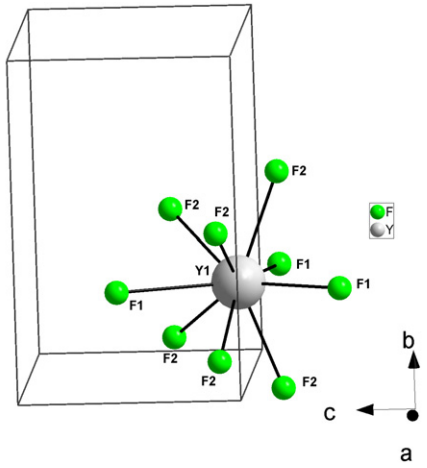

Figure 8. Sketch of the first coordination sphere of Y^{3+} within an elementary cell of the YF_3 structure according to the structure description in [25]. Two different fluorine sites exist in this structure marked as F1 and F2. The fluorine polyhedron can be viewed as consisting of three triangles, the F1-based central one in the plane of Y^{3+} and two F2-based ones on the opposite mirror sites. The symmetry of the yttrium site is further lowered by non-equal distances among the Y and F1 ions, −2.282, 2.287 and 2.538 Å.

(This figure is in colour only in the electronic version)

under excitation at 275 nm (into the Gd^{3+} ^{6}I multiplet) the millisecond decay times of the 310 and 380 nm bands are essentially the same.

The centre responsible for the 380 nm emission is based on the Ce^{3+} ion due to its intrinsic decay time of about 23 ns (see figure 7). However, it seems difficult to characterize this centre simply as 'Ce perturbed' as done before in CeF_3, LaF_3 or GdF_3 matrices [15, 18–20], where the perturber is most probably a single anion vacancy in the first coordination sphere of Ce^{3+}. In the present case the centre concentration is not directly proportional e.g. to the concentration of codoping Me^{2+} ions, see also table 1, which were shown to increase the Ce-perturbed emission in CeF_3 [20] due to an increase of anion vacancy concentration for charge compensation. Instead, it seems to be dependent on the size of the Me^{2+} ion and mutual concentration ratio of Me^{2+} and Ce^{3+} ions. Hence, we prefer to refer to this centre as 'Ce-distorted' to reflect its possibly more complex arrangement and the induced local lattice distortion. The Ce^{3+} ion substitutes the Gd^{3+}(Y^{3+}) cation at the nine-coordinated site of rather low local symmetry (Wyckoff symbol 4*c*, site symmetry *.m.*); see the sketch in figure 8. Due to the larger ionic radius of Ce^{3+} and the low symmetry of the site, an extended Ce^{3+} excited state relaxation and resulting large Stokes shift is expected in the situation when some of the surrounding anions will be missing. However, as mentioned above, the presence of a single fluorine vacancy cannot explain the 380 nm emission intensity variation over the sample set studied. Hence, correlated space location of the Me^{2+} ion and the compensating fluorine vacancy in the second and first coordination sphere of Ce^{3+}, respectively, is tentatively proposed as a possible configuration for the Ce-distorted centre in the YF_3–GdF_3 host. The existence of spatially correlated impurity ion–vacancy pairs is well evidenced in alkali halides when the charge compensation is needed (e.g. Pb^{2+}-doped alkali chlorides or bromides) [26] and the probability of their space correlation increases with the ionic character of the compound. The ability of the lattice to accommodate such a complex centre might be dependent on the concentrations of both the Ce and Me ions and the size of the latter as well.

Maximum concentrations of the Ce-distorted centre judged from the 380 nm band intensity in radioluminescence spectra (figure 2) are obtained for the doped ion compositions as Ca0.5–1%Ce3–5% and Sr3%Ce3%. They can be estimated from the additional absorption around 290 nm (figure 1) in the following way. From the absorption spectrum of the thin (0.3 mm) Ce1%Sr13%Gd86%$F_{2.87}$ sample the absorption coefficient in the lowest 4f–5d^1 transition of the regular Ce^{3+} centre peaking at 250 nm becomes about 13.5 mm^{-1}. The additional absorption coefficient at 290 nm in the Ca1%Ce3%Y60%$GdF_{2.99}$ samples is 0.064 mm^{-1} and this wavelength can be reasonably ascribed to the maximum of the lowest 4f–5d^1 absorption transition of the Ce-distorted centre. If we admit the same oscillator strength for both the regular and Ce-distorted centres and neglect inhomogeneous broadening of the latter, by comparison of the above determined absorption coefficients, we get the concentration of the Ce-distorted centre of about 50 ppm. Let us consider the characteristics of the energy transfer process between the 310 and 380 nm bands in more detail. A striking feature of the 310 nm donor decays at room temperature is their perfect single-exponential character (examples in figure 5) for any concentration of the Ce-distorted acceptor centres. Such a feature together with significant decrease of the decay time value in the case of the highest concentrations of Ce-distorted centres (from about 13–14 ms in Y50%GdF_3 or Mg0.5%Ce3%Y55%GdF_3 samples down to about 1.5 ms in Ca1%Ce3%Y60%GdF_3) points to very fast energy migration in the donor Gd sublattice and the so called Stern–Volmer model can be applied [27] to describe the concentration dependence of the donor luminescence decay. In this approximation obtained for the case of rapid energy migration from the Yokota–Tanimoto model [28] the donor decay $I(t)$ is described as

$$I(t) = A \cdot \exp\left[\frac{-t}{\tau_{\mathrm{rad}}}\left\{1 + \frac{c_{\mathrm{a}}}{c_{\mathrm{a0}}}\right\}\right], \tag{1}$$

where τ_{rad} stands for the radiative lifetime of the donor emission, c_{a} is the concentration of the acceptor centres and c_{a0} is the so called 'critical concentration' defined as the concentration of acceptors at which the measured decay time is half the donor radiative lifetime, i.e. at which 50% of energy contained in the donor sublattice at $t = 0$ is transferred to the acceptor centres. Measured decay time τ is thus

$$\tau = \frac{\tau_{\mathrm{rad}}}{1 + \frac{c_{\mathrm{a}}}{c_{\mathrm{a0}}}}. \tag{2}$$

We adopt the values for $\tau_{\mathrm{rad}} = 14$ ms. In the sample Ca1%Ce3%Y60%GdF_3 the value of $\tau_{(300\ \mathrm{K})} = 1.47$ ms and $c_{\mathrm{a}} = 50$ ppm. Hence the calculation provides the parameter $c_{\mathrm{a0}} = 6$–7 ppm. Such a low value of critical concentration together with the long radiative lifetime of Gd^{3+} donor emission points to very efficient energy transfer to the acceptor centres with minimum nonradiative losses due to parasitic energy transfer to unspecified traps (defects) in the host lattice. Furthermore, an estimate of the c_{a} concentration in the sample Sr0.1%Ce1%Y55%GdF_3 can be made from the inset of figure 1 ($\sim$17 ppm). Using the calculated critical concentration $c_{\mathrm{a0}} = 6$–7 ppm and equation (2) the 310 nm decay time is calculated within 3.6–4.1 ms for this sample. The experimental value is 3.9 ms, which perfectly matches the calculated range.

The temperature dependence of the emission spectra of Ca1%Ce3%Y60%GdF_3 sample under 272 nm excitation, figure 4, deserves another comment as the total intensity (spectrum integral over 300–500 nm) is increasing with the temperature up to about 360 K and the reason is not obvious. Around 270–275 nm there is an overlap of the Gd^{3+} ^8S–^6I and regular Ce^{3+} 4f–5d^1 transitions. The latter absorption transition peaks around 250 nm, its halfwidth is broadened with increasing temperature and the absorption coefficient at 272 nm and 300 K is about 1.5 mm^{-1}. In this situation the increasing absorbance at 272 nm with temperature will

result in an increased absorption of the excitation energy and total emission intensity as well. Another temperature-dependent process influencing the efficiency of energy transfer towards the Ce-perturbed centres is reflected in the temperature dependence of the 380 nm emission intensity under the 311 nm excitation. In this case, temperature-induced broadening of the lowest excitation peak of the Ce-distorted centre around 290 nm will result in an increased overlap with the 310 nm emission line of the Gd^{3+} donor centres. Therefore, the interaction strength and energy transfer efficiency may be increased in the case when some competitive energy transfer loss exists. Even if we conclude that such processes have minor importance, see above, some losses can be expected, if one compares e.g. the decay times of 310 nm emission in the '380 nm band-free' Y50%GdF_3 and Mg0.5%Ce3%Y55%GdF_3 samples in figure 6.

Despite the highly efficient energy transfer to the Ce-distorted centres in this host, it is worth noting that in the present case the bigger mean Gd–Gd distance as well as low concentration of the acceptor centres result in rather slow luminescence response of the material. In Gd-concentrated fluorides, where one can achieve high concentration of the acceptor centres like $CsGd_2F_7$:Ce [14], it is shown that the Gd^{3+} donor decay time can be shortened to units of microseconds in the case when the Ce^{3+} acceptor centre concentration is above 10%. However, there is an important advantage of the material system we present: exceptionally high Stokes shift of the Ce-distorted centre (about 8000 cm^{-1}) results in the positioning of the emission band at 380–390 nm, which prevents any back energy transfer from the Ce-distorted to Gd^{3+} centres. Bi-directional energy exchange between the Gd sublattice and Ce-based centres was recognized as a problem in $CsGd_2F_7$:Ce [14] as far as time characteristics are considered. To our knowledge, this is the first case of a Ce-based emission centre in a fluoride host which provides the emission band positioned at sufficiently low energy with respect to the $^6P_{7/2}$–^8S emission line of Gd^{3+} to prevent the back energy transfer even at room temperature.

5. Conclusions

Double doping of the YF_3–GdF_3 host by Me^{2+} (Me = Mg, Ca, Sr, Ba) and Ce^{3+} in suitable concentration results in the creation of the Ce^{3+}-distorted centre, the absorption and emission of which is noticeably low energy shifted with respect to the regular Ce^{3+} absorption and emission levels typical for AF_3 hosts (A = La, Lu, Gd, Ce). Its lowest 4f–$5d^1$ absorption band is situated around 290 nm and a high Stokes shift exceeding 8000 cm^{-1} results in the emission band positioned at 380–390 nm. Due to such an energy level arrangement, an efficient energy transfer occurs from the Gd^{3+} sublattice to this centre with no back transfer observed. The Ce^{3+}-distorted centre is tentatively ascribed to the Ce^{3+} ion with the coupled anion vacancy and Me^{2+}-codoped ion in its first and second coordination spheres, respectively. Considerably fast and efficient energy migration was proved within the Gd^{3+}-energy-guiding sublattice and extremely low, about 6–7 ppm, critical concentration of the acceptor Ce^{3+}-distorted centre was calculated. However, for practical application of such materials e.g. like fast scintillators, much higher concentration of the Ce^{3+}-distorted centres with respect to those currently achieved (approximately 50 ppm) is needed.

Acknowledgments

Financial support of the Czech Institutional Research Plan No AV0Z10100521 and MSMT KONTAKT 1P2004ME716 projects together with Estonian Science Foundation grant No 6548 and Japanese Industrial Technology Research Grant Programme 03A26014a from the New

Energy and Industrial Technology Development Organization (NEDO) as well as a Grant in Aid for Young Scientists (A), 15686001, 2003, by the Ministry of Education, Culture, Sports, Science and Technology of the Japanese government (MEXT), is gratefully acknowledged.

References

[1] Kodama N, Yamaga M and Henderson B 1998 *J. Appl. Phys.* **84** 5820
[2] Dorenbos P 2000 *Phys. Rev.* B **62** 15640
[3] Ehrlich D J, Moulton P F and Osgood R M 1980 *Opt. Lett.* **5** 339
[4] Marshall C D, Speth J A, Payne S A, Krupke W F, Quarles G J, Castillo V and Chai B H T 1994 *J. Opt. Soc. Am.* B **11** 2054
[5] Liu Z, Shimamura K, Nakano K, Fukuda T, Kozek T, Ohtake H and Sarukura N 2000 *Japan. J. Appl. Phys.* **39** L466
[6] Nikl M 2000 *Phys. Status Solidi* a **178** 595
[7] Combes C M, Dorenbos P, van Eijk C W E, Pedrini C, Den Hartog H W, Gesland J Y and Rodnyi P A 1997 *J. Lumin.* **71** 65
[8] van 't Spijker J C, Dorenbos P, van Eijk C W E, Jacobs J E M, den Hartog H W and Korolev N 1999 *J. Lumin.* **85** 11
[9] Suzuki H, Tombrello T A, Melcher C L, Peterson C A and Schweitzer J S 1994 *Nucl. Instrum. Methods Phys. Res.* A **346** 510
[10] Nikl M, Nitsch K, Mihokova E, Solovieva N, Mares J A, Fabeni P, Pazzi G P, Martini M, Vedda A and Baccaro S 2000 *Appl. Phys. Lett.* **77** 2159
[11] Dorenbos P, Spijker J C and van Eijk C W E 1997 *Proc. SCINT97 (Shanghai, China, Sept. 1997)* ed Z Yin, P Li, X Feng and Z Xue, Shanghai Branch Press, p 307
[12] Dorenbos P, van't Spijker J C, Frijns O W V, van Eijk C W E, Krämer K, Güdel H U and Ellens A 1997 *Nucl. Instrum. Methods Phys. Res.* B **132** 728
[13] Verweij J W M, Pedrini C, Bouttet D, Dujardin C, Lautesse H and Moine B 1995 *Opt. Mater.* **4** 575
[14] Schaart D R, Dorenbos P, van Eijk C W E, Visser R, Pedrini C, Moine B and Khaidukov N M 1995 *J. Phys.: Condens. Matter* **7** 3063
[15] Blasse G 1982 *Phys. Status Solidi* a **73** 205
[16] Moine B, Dujardin C, Lautesse H, Pedrini C, Combes C M, Belsky A, Martin P and Gesland J Y 1997 *Mater. Sci. Forum* **239–241** 245
[17] Dujardin C, Pedrini C, Garnier N, Belsky A N, Lebbou K, Ko J M and Fukuda T 2001 *Opt. Mater.* **16** 69
[18] Pedrini C, Moine B, Gacon J C and Jacquier B 1992 *J. Phys.: Condens. Matter* **4** 5461
[19] Wojtowicz A J, Balcerzyk M, Berman E and Lempicki A 1994 *Phys. Rev.* B **49** 14880
[20] Nikl M and Pedrini C 1994 *Solid State Commun.* **90** 155
[21] Lammers M J J and Blasse G 1985 *Phys. Status Solidi* b **127** 663
[22] Poort S H M, Meyerink A and Blasse G 1997 *Solid State Commun.* **103** 537
[23] Yoshikawa A, Satonaga T, Kamada K, Sato H, Nikl M, Solovieva N and Fukuda T 2004 *J. Cryst. Growth.* **270** 427
[24] Kamada K, Yosikawa A, Aoki K, Nikl M and Fukuda T 2006 Crystal growth and scintillation properties of Ce and Sr co-doped (Gd, Y)F_3 single crystals *J. Cryst. Growth* submitted
[25] Cheetham A K and Norman N 1974 *Acta Chem. Scand.* A **28** 55
[26] Jacobs P W M 1991 *J. Phys. Chem. Solids* **52** 35
[27] Wright J C 1976 Up-conversion and excited state energy transfer in rare earth doped materials *Radiationless Processes in Molecules and Condensed Phases* ed F K Fong (Berlin: Springer) pp 239–97
[28] Yokota M and Tanimoto O 1967 *J. Phys. Soc. Japan* **22** 779